International Journal of Energy Engineering 2021, 11(1): 9-16
DOI: 10.5923/j.ijee.20211101.02

Determination of the Dynamic Field in the Penstock of the Trois-Gorges Dam by a Numerical Approach

Nkontchou Ngongang François[1], Tchawe Tchawe Moukam[1,*], Tientcheu Nsiewe Max-well[2], Djiako Thomas[3], Djeumako Bonaventure[1], Tcheukam-Toko Dénis[4]

[1]Department of Mechanical Engineering, ENSAI, University of Ngaoundere, Cameroon
[2]Department of Fundamental Sciences, EGCIM, University of Ngaoundere, Cameroon
[3]Department of Mechanical Engineering and Energy, ISTA, University Institute of the Gulf of Guinea, Cameroon
[4]Department of Mechanical Engineering, COT, University of Buea, Cameroon

Abstract This work deals with determining the characteristics of the flow through the penstock of the Three Gorges dam in China. It also allows us to understand the influence of the diameter of the water duct on the modification of the flow structure in the penstock. To achieve our goals, the Eulerian resolution of the Navier-Stokes equations is done by a RANS approach using the FLUENT calculation code. The turbulence model applied is that with two k-ε equations. The results show constant velocities upstream of the dam until approaching the water intake at a distance of about 15m upstream, keeping an asymmetric shape in the different sections constituting the penstock. The maximum velocities are observed on the innerside of the various elbow. Layers of positive pressure are also visible in the penstock away from the walls; suggesting substantially coaxial and positive iso-pressures in high velocity zones, with a maximum directed towards the center of the penstock. This phenomenon thus goes against the "high velocity-low pressure" hypothesis, and may be justified by the geographical arrangement of the penstock, associated with its large diameter.

Keywords Hydroelectric dam, Penstock, Dynamic fields, CFD

1. Introduction

The production of electrical energy by hydroelectric power stations is booming around the world. Of the equipment constituting these structure, the penstock and the turbine constitute sensitive equipment because of their impact on the performance of the entire structure [1]. They are at the origin of more than half of the studies carried out on these master piece according to our research.

This work focuses on penstocks that channel pressurized water to the turbine. They can be mild steel, glass reinforced plastic (GRP), reinforced concrete (RC), wooden staves, cast iron and high density polyethylene (HDPE), etc. However, due to greater applicability and availability, mild steel is the most widely used [2]. For less expensive and rapid studies, researchers use a modern tool that facilitates studies in the field of fluid mechanics.

The CFD for "Computational Fluid Dynamics" allows the study of complex flows encountered in engineering. Its development, with the digital age, now results in enormous possibilities so that it is possible to model the three-dimensional flow [3]. In addition, it offers the possibility of taking an in-depth look at the flow, which helps in understanding complex phenomena. These phenomena may be different depending on the shape of the penstock, or another parameter such as the shape of the water intake.

In this document, we will present studies carried out on the penstock of the Three Gorges dam in China. The main objective in this first document relates to the determination of the hydraulic characteristics observed on the flow through the penstock of this dam. Thus, we will present cross sections of the penstock at very precise distances, in order to observe the fluid layers crossing the penstock to the turbine inlet.

2. Material and Methods

2.1. Assumption of Calculation Domain

The model of our penstock is shown in Figure 1 below for a maximum flow rate of 970 m^3/s. The structure is made up of three pipe sections linked together by elbows:

- The first section is located between the water intake and the first elbow;
- The second section is the part which is found between the two elbows;

* Corresponding author:
christophetchawe@yahoo.fr (Tchawe Tchawe Moukam)
Received: Aug. 23, 2021; Accepted: Sep. 20, 2021; Published: Oct. 30, 2021
Published online at http://journal.sapub.org/ijee

- The third section is the one between the second elbow and the turbine inlet.

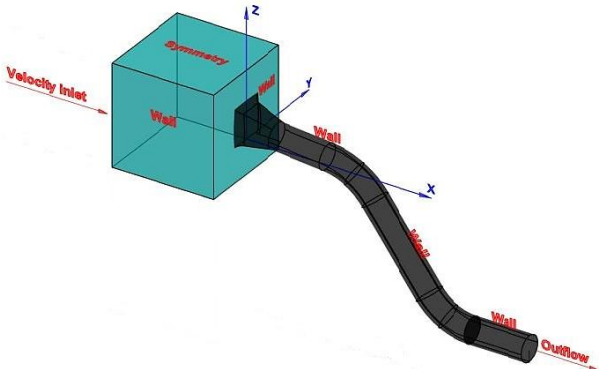

Figure 1. Three-dimensional model with boundary condition

The turbulence model used is k-ε Realizable because it is well suited to boundary layers with a strong adverse pressure gradient, to strong curvature and vortex flows and a considered isotropic. The second order equations are solved with the velocity-pressure coupling method SIMPLEC and a convergence criterion of 10^{-6}. The function near walls function considered is the standard wall function, and the discretization scheme is Body Force Weighted. The approach flow is stationary and the turbulence is isotropic.

2.2. Governing Equations

The flow is incompressible and isothermal with constant viscosity, and can be described by the velocity and pressure field governed by the Navier-Stokes equations [4] quoted by [5]. The fluid is assumed to be a Newtonian fluid. We have:

$$\frac{\partial U_i}{\partial U_j} = 0 \tag{1}$$

The dynamic conservation is:

$$\frac{\partial U_i}{\partial t} + \frac{\partial (U_j U_i)}{\partial x_j} = \frac{1}{\rho}\left(-\frac{\partial p}{\partial x_i} + \frac{\partial \tau_{ij}}{\partial x_i}\right) \tag{2}$$

where $\boldsymbol{U_i}$ represents the velocities in $\boldsymbol{x_i}$ coordinate directions; **p** is the static pressure load, **ρ** the constant density, and $\boldsymbol{\tau_{ij}}$ the viscous stress tensor. For a Newtonian fluid:

$$\tau_{ij} = \mu\left(\frac{\partial U_i}{\partial x_j} + \frac{\partial U_j}{\partial x_i}\right) \tag{3}$$

In the flows, the variations are too rapid to be described in time and space. Velocity details are lost. We can adopt the following decomposition for the pressure and the velocity:

$$u_i = \overline{u_i} + u_i^{'} \tag{4}$$

where $\overline{u_i}$ and $u_i^{'}$ are the average components of the fluctuating velocity $(i = 1, 2, 3)$. In the same way for the pressure and the other scalar values:

$$\phi = \bar{\phi} + \phi^{'} \tag{5}$$

Where ϕ represents a scalar such as pressure, energy, or other concentration.

Substituting expressions of this form for the flow variables in the instantaneous continuity and momentum equations while taking a time average, we obtain the average momentum equations. They can be written in the form of Cartesian tensor:

$$\frac{\partial \rho}{\partial t} + \frac{\partial}{\partial x_i}(\rho u_i) = 0 \tag{6}$$

$$\frac{\partial}{\partial t}(\rho u_i) + \frac{\partial}{\partial x_i}(\rho u_i u_j) = -\frac{\partial p}{\partial x_i} + \frac{\partial}{\partial x_j}\left[\mu\left(\frac{\partial u_i}{\partial x_j} + \frac{\partial u_j}{\partial x_i} + \frac{2}{3}\delta_{ij}\frac{\partial u_l}{\partial x_l}\right)\right] + \frac{\partial}{\partial x_j}\left(-\rho\overline{u_i^{'}u_j^{'}}\right) \tag{7}$$

Additional terms now appear that represent the effects of turbulence. The Reynolds stress $\rho\overline{u_i^{'}u_j^{'}}$, must be modeled to close the equation. The closing of the equation uses Boussinesq's approximation [6]:

$$-\rho\overline{u_i^{'}u_j^{'}} = \mu\left(\frac{\partial u_i}{\partial x_j} + \frac{\partial u_j}{\partial x_i}\right) - \frac{2}{3}\left(\rho k + \mu_t \frac{\partial u_i}{\partial x_i}\right)\delta_{ij} \tag{8}$$

The model of the transport equations for k and ε is:

$$\frac{\partial}{\partial t}(\rho k) + \frac{\partial}{\partial x_i}(\rho k U_j) = \frac{\partial}{\partial x_i}\left[\left(\mu + \frac{\mu_t}{\sigma_k}\right)\frac{\partial k}{\partial x_j}\right] + G_k + G_b + \rho\varepsilon + Y_M + S_k \tag{9a}$$

$$\frac{\partial}{\partial t}(\rho\varepsilon) + \frac{\partial}{\partial x_j}(\rho\varepsilon U_j) = \frac{\partial}{\partial x_j}\left[\left(\mu + \frac{\mu_t}{\sigma_\varepsilon}\right)\frac{\partial \varepsilon}{\partial x_j}\right] + \rho C_1 S_\varepsilon + \rho C_2 \frac{\varepsilon^2}{k + \sqrt{\nu\varepsilon}} + C_{1\varepsilon}\frac{\varepsilon}{k}C_{3\varepsilon}G_b + S_\varepsilon \tag{9b}$$

where: $C_1 = \max\left[0{,}43\frac{\eta}{\eta+5}\right]$; $\eta = S_\varepsilon^k$; $C_{3\varepsilon} = \tanh\left[\frac{v}{u}\right]$

$\boldsymbol{C_{3\varepsilon}}$ represents the degree of influence of volume forces, $\boldsymbol{v}$ is the component of the flow velocity parallel to the gravitational vector, and $\boldsymbol{u}$ is the component of the flow velocity perpendicular to the gravitational vector.

In these equations, $G_k = -\rho\overline{u_i^{'}u_j^{'}}\frac{\partial u_j}{\partial x_i}$ represents the generator term of the kinetic energy of turbulence due to the mean of the calculated velocity gradient, $G_b = \beta g_i \frac{\mu_t}{P_{rt}}\frac{\partial T}{\partial x_i}$ is the generator term of the kinetic energy of turbulence due to the volume forces, Y_M represents the fluctuation of the expansion in compressible turbulence. C_1 and C_2 are their constants. σ_k et σ_ε are the turbulent Prandtl numbers for k and ε respectively [7] quoted by [1]. S_k and S_ε are user-defined terms.

The turbulent viscosity is given by:

$$\mu_t = \rho C_\mu \frac{k^2}{\varepsilon} \tag{10}$$

The difference between the three models is in the term of C_μ which is given by:

$$C_\mu = \frac{1}{A_0 + A_S\frac{kU^*}{\varepsilon}} \tag{11}$$

The constants are given by:

$A_0 = 4{,}04$; $A_S = \sqrt{6}cos\phi$

$C_{1\varepsilon} = 1{,}44$; $C_2 = 1{,}9$; $\sigma_k 1{,}0$; $\sigma_\varepsilon = 1{,}2$

3. Results and Discussion

3.1. Mesh Geometry

Solving the equation of conservation of mass, momentum and energy equations requires the use of boundary conditions for each dependent variable. The velocity conditions at the walls and at the openings are shown in Figure 1 above. The nearing flow is always assumed to be stationary.

To better understand the evolution of the flow structure in the penstock, we have divided each of the sections into three parts as we will see below.

We see that the velocity is constant upstream of the dam until near the water intake, at a distance of about 15m upstream. After this distance, we see a change in the flow structure under the influence of the water intake.

The legends presented on the fields correspond to the average values existing in the entire structure.

As the modeling is three-dimensional, Figures 2 below show us a longitudinal section (median plane) of the mesh used in the study. We have in this figure numbers corresponding to the different portions studied.

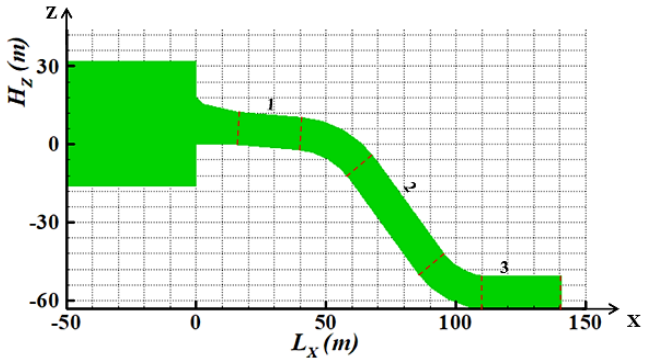

Figure 2. Structure of the mesh with different portions studied

We bring out in Figure 3 the mean sensitivities of the meshes corresponding to four mesh structures that have been the subject of the study in this work.

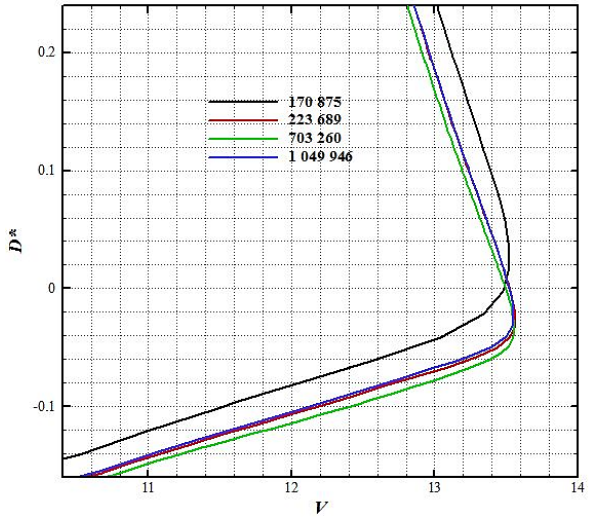

Figure 3. Mesh sensitivity

3.2. Velocity Fields

From the study of the sensitivity of the mesh, we find that the mesh no longer has a very large impact on the profiles obtained from 223,600 cells as shown in Figure 3 above. However, we opted for the more dence mesh, of 1049946 cells.

To better understand the evolution of flow layers in the pipe so we be located in relation to each section distance, a longitudinal outline of the part of the structure studied is presented. This longitudinal section corresponds to the dynamic field studied, namely the velocity field and the pressure field.

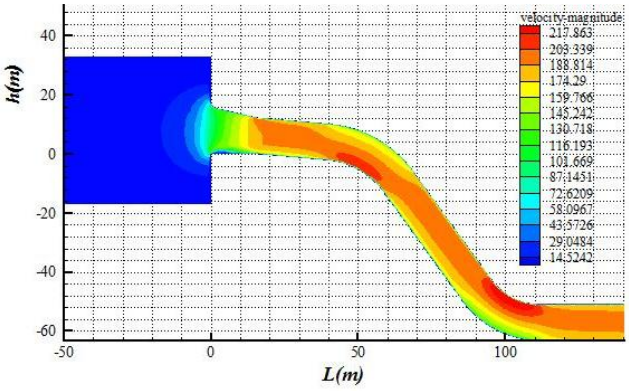

a)

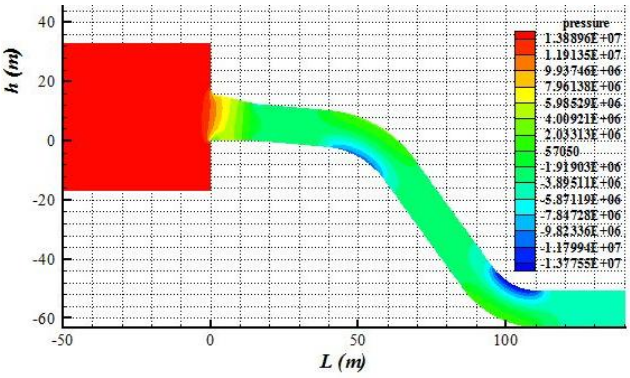

b)

Figure 4. Velocity (a) and pressure (b) field at y = 0 m

The velocity increases as we approach the penstock. We then observe layers of high velocity crossing the penstock with an asymmetric shape to the axis of the pipe in different sections. The maximum velocities are on the innerside of the various curves, with a heavier layer at the second elbow.

For the pressure field, the high pressure layers are observed in the upstream zone (reservoir) at the water intake. Similarly, low pressure layers are observed in the innerside of each curve. However, we also see layers of positive pressure in the penstock away from the walls. For an in-depth observation of these different phenomena, we will subsequently make cross-sections on each section of the penstock.

These three transects better reflect the flow evolution in this section of the penstock. Observing Figure 5a and at the

start of this portion (x = 15m), the maximum velocities are observed near the walls in separate layers; the vast majority being on the upper side. As we move forward in the pipe.

Thus, we have opted to make three cuts for each section. The entrance to the water intake is located at a distance of x=0m.

3.2.1. First Section

The three cuts of this section are located at the following respective distances: x = 15 m, x = 28 m which approximately represents the middle, and x = 40 m for the exit as shown in Figures 5a and 5b below.

These layers concentrate towards the center of the penstock as we can see at the distance x = 28m. At the exit of this portion (entry of the elbow), this curve has an elliptical shape, and is pressed against the bottom wall of the pipe. Note that from the fields, we seem to be in the presence of three layers in the cuts presented.

Figure 5b shows the pressure field. At x = 15 m, we observe a pressure force towards the center of the pipe, thus reflecting the effect of the concentration of the intake on the inlet flow. Its quadrilateral shape represents the shape of the socket. The flow in its evolution towards the elbow presents a maximum pressure towards the center of the pipe, thus limiting the hypothesis of high pressure low velocity.

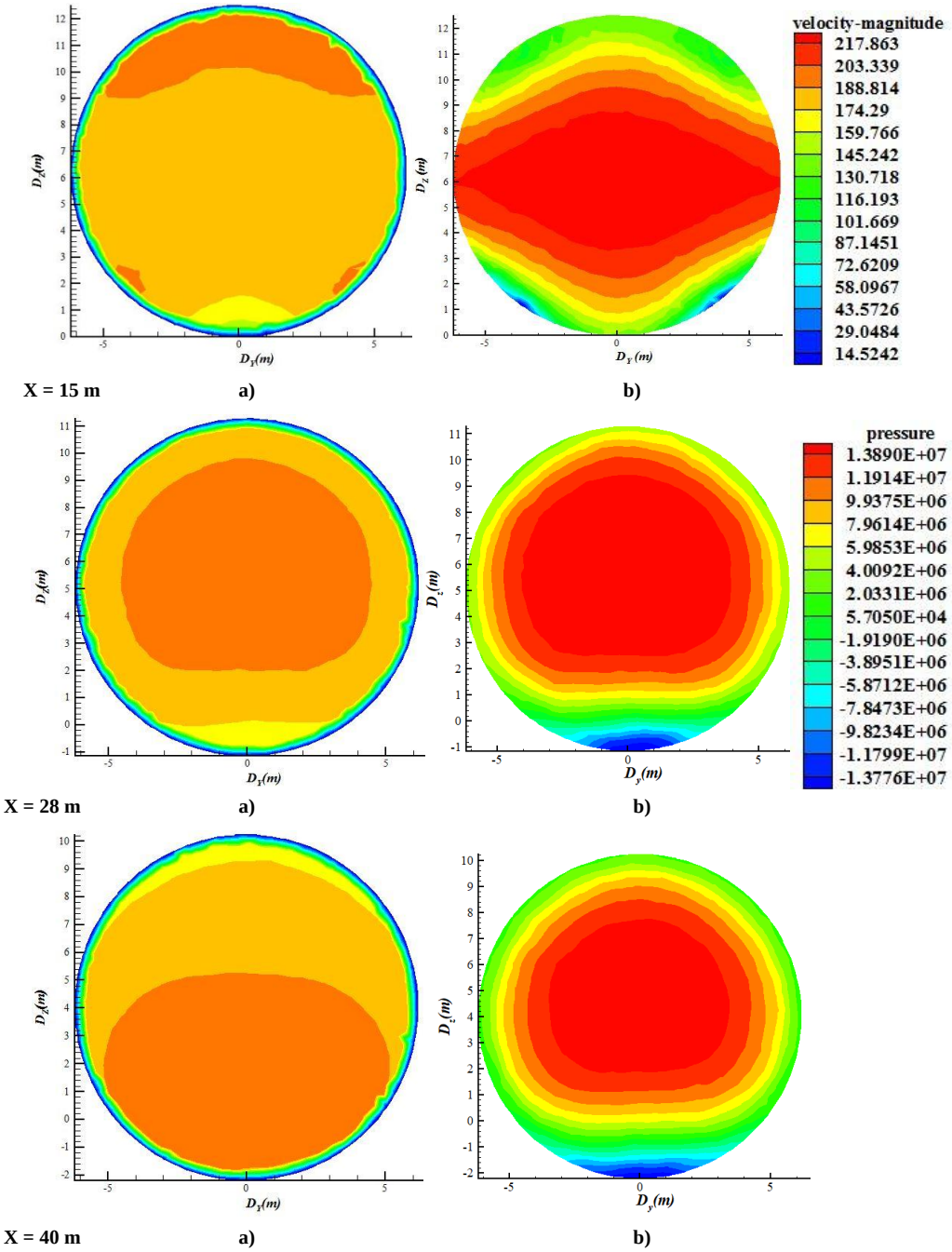

Figure 5. Velocity (a) and pressure (b) field in section 1

At the exit of the first elbow, we seem to be in the presence of two layers, with the high velocity layer observed on the bottom wall as shown in figure 6a, at the distance x = 57m.

We subsequently observe substantially coaxial iso-pressures with a maximum, directed towards the center of the penstock. However at the distance x = 40m, the low pressure layer is observed on the bottom wall.

3.2.2. Second Section

For this section, the three cuts are placed at the respective distances x = 57m (for the entrance), x = 70 m (for the middle) and x = 95 m (for the exit or the entry into the second elbow).

Moving towards the middle of the portion, we seem to be in the presence of 3 layers, with the high velocity layer observed towards the upper part in the penstock. At x = 95m, we observe several fluid layers, with a high velocity layer practically stuck to the upper wall (ceiling) of the penstock. In figure 6b, we observe the same iso-pressure as noted previously, with the layers of high pressure in the upper part of our penstock (at x = 57m). As they move away in the section, these layers remain at the top of the penstock, keeping its ovoid shape. Once again, we observe non-zero iso-pressures in high velocity zones; which again goes against the high velocity-low pressure phenomenon.

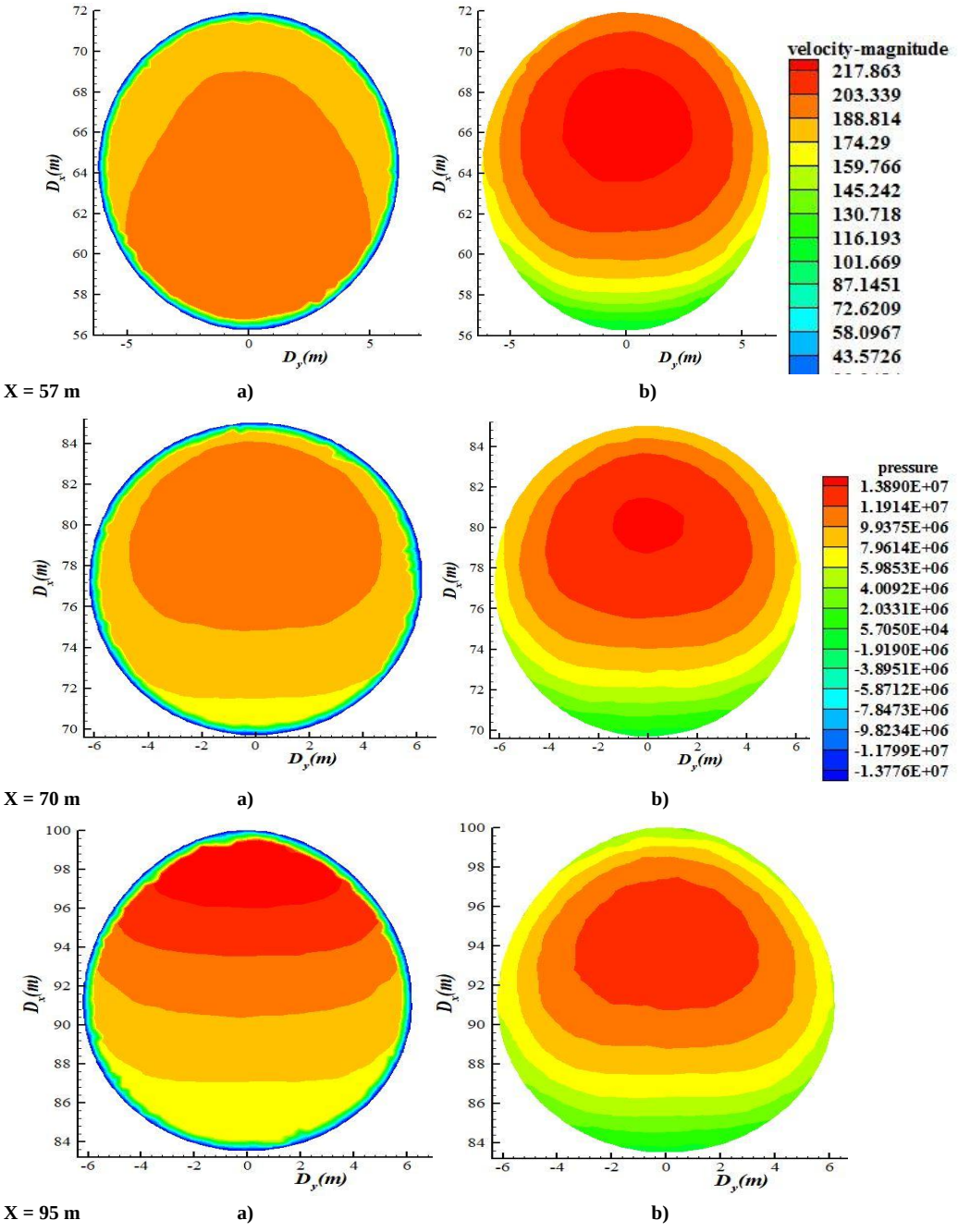

Figure 6. Velocity (a) and pressure (b) field in section 2

The velocity fields present us with several fluid layers at the exit of the second elbow as we can see in figure 7a above, at x = 112m. As you approach the turbine, the flow becomes symmetrical as shown in the figure above at x = 140m.

This new phenomenon can be justified by the geographical disposition of the penstock, associated with its large diameter. However, this is one of the objects of an ongoing study.

3.2.3. Third Section

As with the previous sections, the distances here are x = 112 m (for the entrance), x = 125 m (for the middle) and x = 140 m (for the exit). It should be noted that this section has the particularity of being arranged horizontally.

Regarding the pressure fields, we make the same remark on the position of the high pressure layers. These once again show maximum pressure in the wake of high velocities.

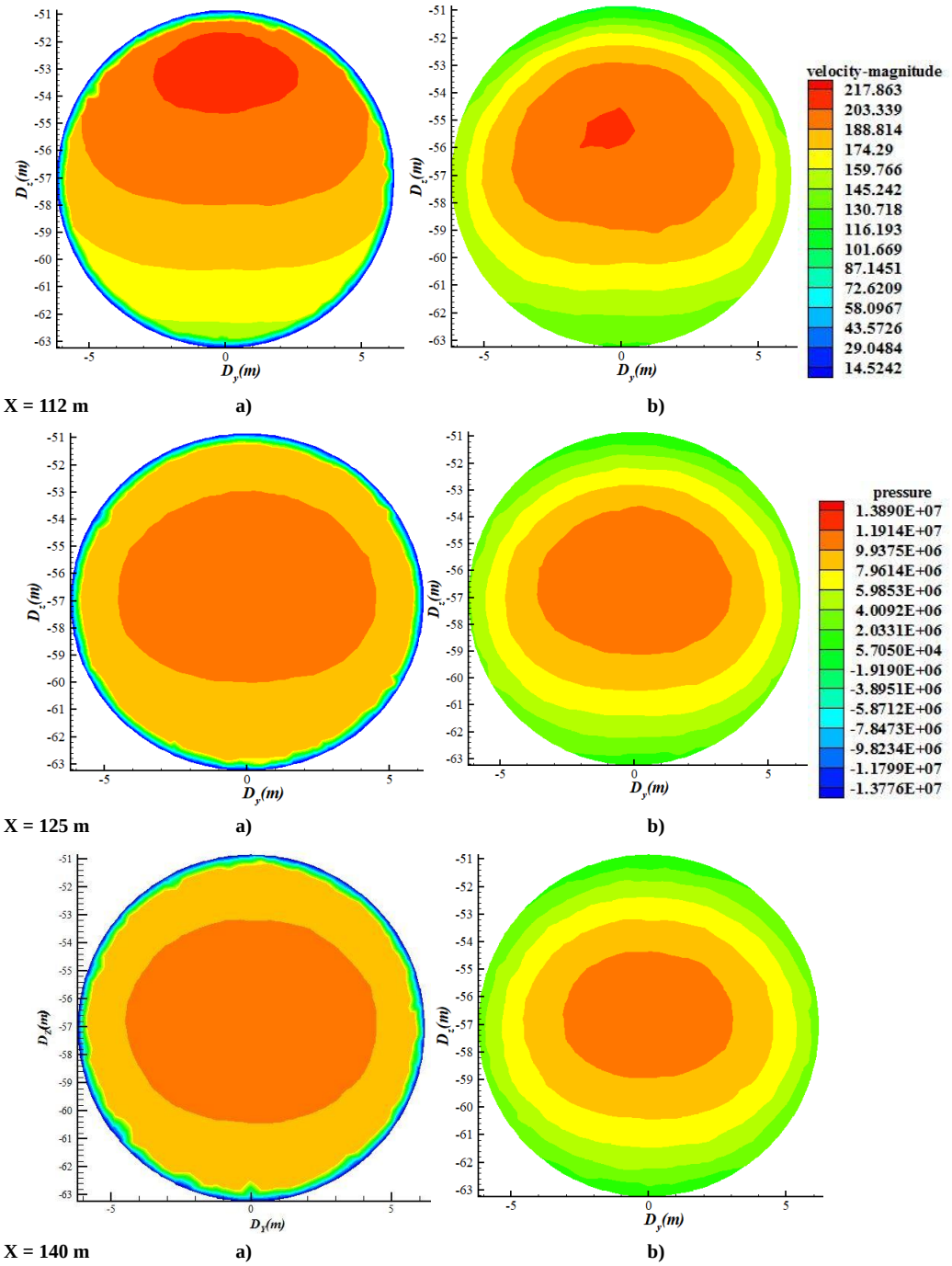

Figure 7. Velocity (a) and pressure (b) field in section 3

3.3. Comparative Studies

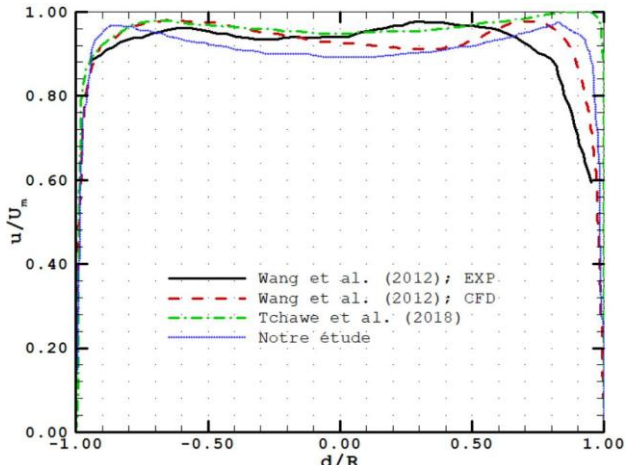

Figure 8. Penstock velocity profile for Wang et *al.* [8], Tchawe et *al.* [9], and this study

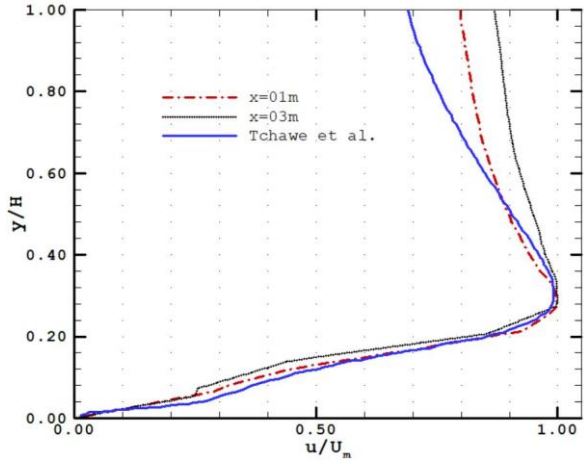

Figure 9. Profile of velocities near the wall for the present study and that of Tchawe et *al.* [9]

Several studies are carried out on penstocks and these on various aspects. However, the structure of the flow remains one of the unknown parameters of the operation of the structure, because it is difficult to observe. As the interest of these studies relates to improving the performance of the entire structure, they are therefore essential on such a structure having been the subject of enormous expenditure and being classified as a risk structure. It is with this logic that Wang et *al.* [8] studied the velocity of the flow in the penstock entrance by the ultrasonic method in the Three Gorges dam. We compare our results with those obtained within the framework of this work as shown in the figure below.

The arrangement of their probes may explain the error observed on the curves. However, from the results obtained within the framework of this work, including that presented in Figure 5 above, we validated our model. We then compared the flow structure upstream of the intake with that obtained in a previous work; this conforts us in the model used as we can see in the figure 6.

The velocity profiles are consistent towards the lower wall, with a peak observed in the same interval. The difference observed towards the upper part of the profiles is justified by the modifications made to the configurations of the structure.

In order to present the closeness at the level of the dynamic field, we compared our study with that of Adamkowski et *al.* (2009) [10], as shown in Figures 10a and 10b below. The goal in their studies was to measure flow using the pressure-time method in a three-section curved penstock like ours, but with a reduced diameter and longer length. It was equally question to evaluate the results obtained numerically on these structure.

Thus, the general flow structure is found on both studies with the high velocity layers near the walls of the intake, folded towards the upper part in the second section and concentrated towards the innerside on each elbow. Likewise, these layers are located towards the axis of the pipe at the exit of the penstock in both researches. These observations are only possible thanks to the numerical approach which allows us to visualize the structure of the flow at each point in the pipe. According to ASME, having fully developed turbulent motion requires a straight line at least 10 times the diameter of the pipe; which is not the case in the two studies.

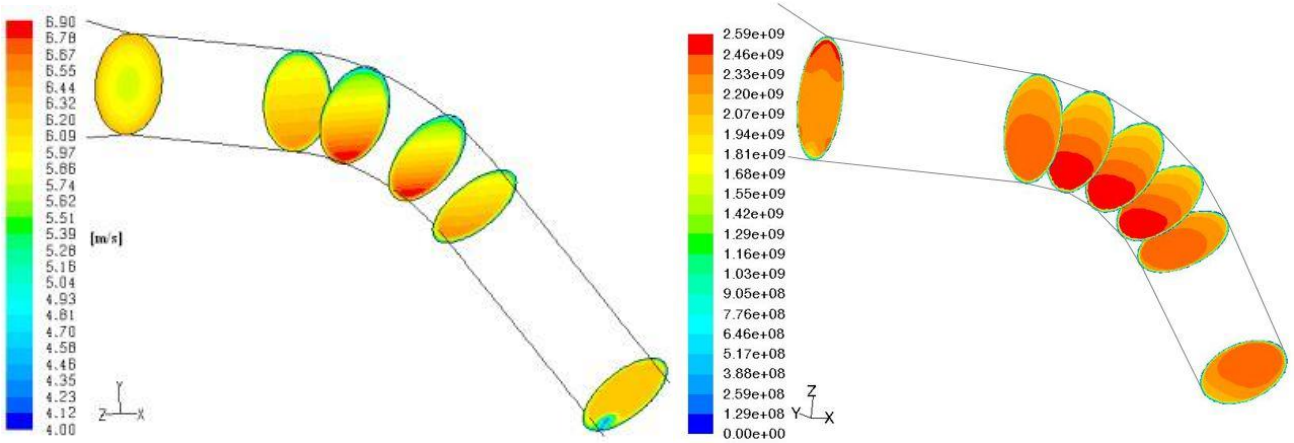

a) **b)**

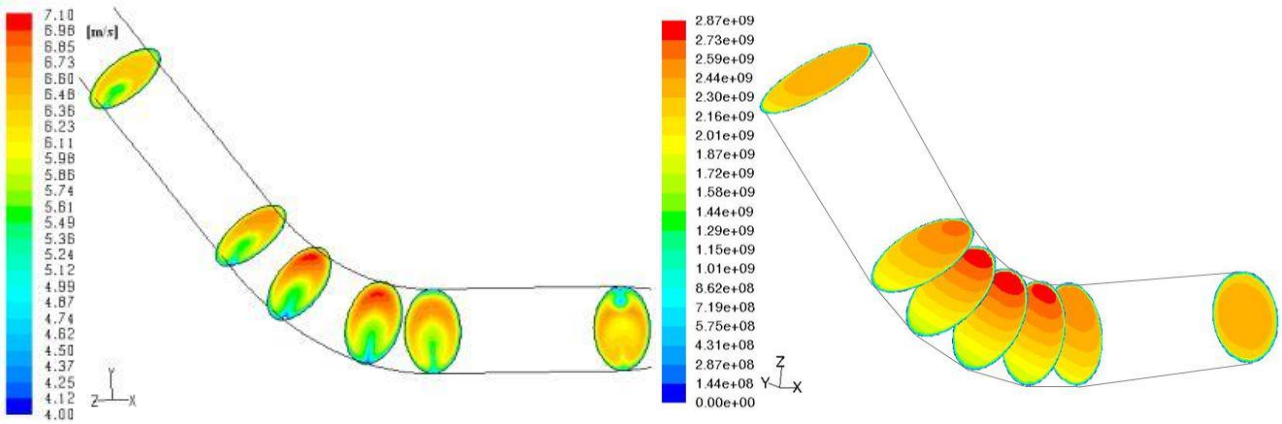

a) **b)**

Figure 10. Velocity field in driving for Adamkowski et *al.* [10] (a), and the present study (b)

4. Conclusions

For us in this work, it was question to determining the dynamic field in the penstock of the Three Gorges dam in China, the objective being to determine the structure of the flow in this pipe using a numerical approach. We have therefore chosen the FLUENT calculation code, which is the most widely used in the world of hydraulic and particularly in hydroelectric dams. From the results obtained, we observe the constant velocity upstream of the dam until near the water intake at a distance of about 15m upstream. Its structure retains its asymmetric character in the different sections that constitute driving with maximum velocitys on the innerside of the different elbow. We also observed layers of non-zero pressure in the penstock, far from the walls; substantially coaxial and positive iso-pressures in high velocity zones, with a maximum directed towards the center of the penstock. A phenomenon that still goes against the high velocity-low pressure hypothesis. This new phenomenon can be justified by the geographical arrangement of the penstock, associated with its large diameter.

ACKNOWLEGDEMENTS

A special acknowledge to the University Institute of the Gulf of Guinea-Cameroon and its Founder Mr Louis Marie DJAMBOU (rest in peace) for his contribution in the development of this work.

REFERENCES

[1] Tchawe T., (2019), "Etude et caractérisation du frottement turbulent dans la conduite forcée et dans le barrage de prise d'eau d'une station hydroélectrique: cas des barrages du Cameroun". Thèse en Génie Mécanique et Productique / Ingénierie des Equipements et Productique, Université de Ngaoundéré.

[2] Singhal M. K. & Kumar A., (2015), "Optimum Design of Penstock for Hydro Projects". *International Journal of Energy and Power Engineering*, Vol. 4, No. 4, 2015, pp. 216-226.

[3] Wilson D. Turbulence modeling for CFD. DCV industries, 2nd Edition, 1998.

[4] Von Karman T., (1934), "The fundamentals of the statistical theory of turbulence". *Journal of Aeronautical Science*, 4, 131-138.

[5] Tchawe T., Djiako T., Kenmeugne B., Tcheukam-Toko D., (2018), "Numerical Study of the Flow Upstream of a Water Intake Hydroelectric Dam in Stationary Regime ". *American Journal of Energy Research*, 2018, Vol. 6, No. 2, 35-41.

[6] Boussinesq, (1877), "Théorie de l'écoulement tourbillonnant et tulmultueux des liquides". Paris, 1897.

[7] Prandtl, (1932), "Ergebnisse Göttingen". 1932, 4, p. 18.

[8] Wang C., Meng T., Hu H., Zhang L., (2012), "Accuracy of the ultrasonic flow meter used in the hydroturbine intake penstock of the Three Gorges Power Station". *Flow Measurement and Instrumentation*, 25: 32–39.

[9] Tchawe T., Djiako T., Kenmeugne B., Tcheukam-Toko D., (2018), "Numerical study of flow in the water inlet of the penstock of a hydroelectric dam", *International Journal of Current Research*, Vol. 10, Issue, 07, pp.71061-71066, July, 2018.

[10] Adamkowski A., Krzemianowski Z. & Janicki W., (2009), "Improved Discharge Measurement Using the Pressure-Time Method in a Hydropower Plant Curved Penstock". *Journal of Engineering for Gas Turbines and Power*, vol. 131, pp.6.

[11] Fluent (2006). User manual 6.3.26.